BNL-226001-2024-JAAM

B--N-Bond-Embedded Triplet Terpolymers with Small Singlet-Triplet Energy Gaps for Suppressing NonRadiative Recombination and Improving Blend Morphology in Organic Solar Cells

B. Pang, R. Li

To be published in "Advanced Materials"

February 2023

Photon Sciences

Brookhaven National Laboratory

U.S. Department of Energy

USDOE Office of Science (SC), Basic Energy Sciences (BES)

DISCLAIMER

WILEY-VCH

B-N Bond Embedded Triplet Terpolymers with Small Singlet-Triplet Energy Gaps for Suppressing Non-Radiative Recombination and Improving Blend Morphology in Organic Solar Cells

Bo Pang, Chentong Liao, Xiaopeng Xu, Shaoqian Peng, Jianlong Xia,* Yuanyuan Guo, Yuan Xie, Yuting Chen, Chunhui Duan, Hongbin Wu,* Ruipeng Li, and Qiang Peng**

B. Pang, C. T. Liao, Dr. X. P. Xu, Dr. L. Y. Yu, Prof. Q. Peng
School of Chemical Engineering and State Key Laboratory of Polymer Materials Engineering, Sichuan University, Chengdu 610065, P. R. China. Email: xpxu@scu.edu.cn; qiangpeng@scu.edu.cn

S. Q. Peng, Prof. J. L. Xia
School of Chemistry, Chemical Engineering and Life Science, Wuhan University of Technology, No. 122 Luoshi Road, Wuhan 430070, P. R. China. Email: jlxia@whut.edu.cn

Dr. Y. Y. Guo
Division of Physics and Applied Physics School of Physical and Mathematical Sciences, Nanyang Technological University, 21 Nanyang Link, Singapore 637371, Singapore.

Prof. C. H. Duan, Y. Xie, Y. T. Chen, Prof. H. B. Wu
Institute of Polymer Optoelectronic Materials and Devices, State Key Laboratory of Luminescent Materials and Devices, South China University of Technology, Guangzhou 510640, P. R. China. Email: hbwu@scut.edu.cn

Dr. R. P. Li
National Synchrotron Light Source II Brookhaven National Lab, Suffolk, Upton, NY 11973, USA.

Keywords: organic solar cells; triplet terpolymers; B-N bond; singlet-triplet energy gap; non-radiative recombination

Suppressing the photon energy loss (E_{loss}), especially the non-radiative loss, is of importance to further improve the device performance of organic solar cells (OSCs). However, typical π-conjugated semiconductors possess a large singlet−triplet energy gap (ΔE_{ST}), leading to a lower triplet state than charge transfer state and contributing to a non-radiative loss channel of photocurrent by triplet state. Herein, a series of triplet polymer donors were developed by introducing a BNIDT block into the PM6 polymer backbone. The high electron affinity of BNIDT and the opposite resonance effect of B-N bond in BNIDT resulted in the lowered highest occupies molecular orbital (HOMO) and the largely reduced ΔE_{ST}. Moreover, the morphology of the active blends was also optimized by fine-tuning the BNIDT content. Therefore, the non-radiative recombination *via* the terminal triplet loss channels and morphology traps was effectively suppressed. The PNB-3:L8-BO device exhibited both small ΔE_{ST} and optimized morphology, favoring the more efficient charge transfer and transport. Finally, the simultaneously enhanced V_{oc} of 0.907 V, J_{sc} of 26.59 mA cm^{-2}, and FF of 78.86% contributed to a champion PCE of 19.02%. Therefore, introducing B-N bond into the benchmark polymers is a possible avenue toward higher-performance of OSCs.

1. Introduction

Organic solar cells (OSCs) are a promising next generation photovoltaic technology due to their light weight, solution processability, and prospect in fabricating large-scale flexible devices.[1-3] Over the past years, great efforts have been devoted to developing narrow bandgap nonfullerene acceptors (NFAs),[3-7] wide bandgap polymer donors,[8-11] sophisticated active layer morphology optimizing techniques,[12-14] and advanced device structures.[15-17] Thus, significant strides have been made in device performance with the power conversion efficiencies (PCEs) over 19% realized in state-of-the-art OSCs.[11, 17-25] Nevertheless, the performance of OSCs still lags behind that of inorganic or perovskite solar cells due to the relatively large photon energy loss (E_{loss}).[26] As established, the E_{loss} can be divided into radiative loss and non-radiative loss.[27-28] NFAs featured with fused-ring backbones possess

long-range π-π stacking, strong electronic coupling, and extraordinarily low tail states, which enable minimizing the energy offset and maintaining a barrier-less exciton dissociation.[29] In this sense, there is almost no room to further lower the radiative loss of NFA-based OSCs.[30] However, OSCs often suffer from high non-radiative loss due to the relatively large energetic disorder of organic semiconductors.[27] For instance, PM6:L8-BO, which is one of the best blend systems, still showed a relative high non-radiative loss of 0.22–0.24 eV in OSCs.[31-32] In this regard, to further improve the performance of OSCs, it is essential to develop effective approaches to minimize the non-radiative recombination loss.

For the non-radiative recombination in OSCs, it can be geminate or non-geminate and includes recombination through triplet states, structural defects or morphology traps, etc.[33] The migration of free charges (holes and electrons) in the donor (D) or acceptor (A) domains may encounter non-geminate or bimolecular recombination at the D/A interfaces, with either singlet (^{1}CT) or triplet (^{3}CT) character in a ratio of 1:3, following the spin statistics.[34] The ^{1}CT and ^{3}CT polarons can recombine or dissociate again into free charge carriers. The NFA-based OSCs typically have a small CT driving force ($\Delta E_{CT} = E_{S1} - E_{CT}$, where E_{S1} and E_{CT} are the S_1 and CT energies, respectively), the geminate recombination of ^{1}CT state to the ground state (S_0) can be largely suppressed.[34-35] Most π-conjugated semiconductors possess a large singlet−triplet energy gap ($\Delta E_{ST} = E_{S1} - E_{T1} \approx 0.7$ eV, where E_{T1} is the triplet (T_1) excitation energy),[34] thus leading to a much lower E_{T1} than E_{CT}. In this sense, ^{3}CT can relax to the lower-lying T_1 (recombination from ^{3}CT to S_0 is spin-forbidden), but the thermalization of T_1 back to ^{3}CT is limited. The decay of T_1 to S_0 *via* intersystem crossing (ISC) and triplet charge annihilation can contribute a major terminal loss channel of photocurrent.[34, 36] Triplet excitons have been evidently observed and dominated the ΔE_3 in the NFA-based OSCs.[37] Therefore, for the purpose of lowering the E_{loss} and charge recombination, it is of great importance to develop new semiconductors with minimized ΔE_{ST}. Recent studies have shown that the ΔE_{ST} of A-D-A and A-DA′D-A type NFAs (*ie.*, IT-4F and Y6) can be effectively reduced by end-group π-π

stacking.[37] Moreover, because of strong electronic coupling and small ΔE_{CT}, the CT states become hybridized with the local excitation (LE) states, favoring the charge generation through direct population of thermalized CT states upon illumination and thus the lower ΔE_3 by enhanced radiative rates.[37] In contrast, there is hardly any high-performance wide bandgap (WBG) polymer donors possess a small ΔE_{ST} reported in the OSC field to match the above NFAs so far. Most recently, Duan et al.[38] developed a novel WBG polymer featuring B-N bond and small ΔE_{ST} for high performance OSCs. The opposite resonance effect between boron and nitrogen atoms effectively separated the frontier energy levels, thus leading to the small ΔE_{ST} and reduced recombination loss.[38] The resulting polymer PBNT-BDD exhibited a comparable PCE to the benchmark polymer PM6 (16.1% *vs* 16.0%) at a lower E_{loss} (0.45 eV *vs* 0.50 eV). In this regard, it is meaningful to take advantage of the opposite resonance effect of B-N bond to develop WBG triplet polymers to lower the ΔE_{ST} and further reduce the non-radiative recombination loss for higher performance OSCs.

In this work, we report the design and synthesis of a series of WBG triplet polymers, namely PNB-1, PNB-3, and PNB-5, by combining PM6 and B-N bond for high-performance OSC applications (Scheme 1). In addition to deepening the highest occupied molecular orbital (HOMO) level and increasing the absorption at longer wavelength range, the introduction B-N bond into the PM6 polymer backbone led to a smaller ΔE_{ST} (0.2–0.3 eV) than the ΔE_{CT} (0.48–0.49 eV) of the corresponding random terpolymers. Therefore, the non-radiative recombination *via* the terminal triplet loss channels was effectively suppressed. As a result, the simultaneously enhanced open circuit voltage (V_{oc}) of 0.907 V, short current density (J_{sc}) of 26.59 mA cm^{-2} and fill factor (FF) of 78.86% contributed to the improved PCE of 19.02%. To our best knowledge, this is the best record for the binary blend OSCs using random terpolymers as the electron donors (**Table S1**). Our results indicated that introducing B-N bond into the benchmark polymers should be a possible avenue toward high-performance of OSCs with further lowered E_{loss} and charge recombination.

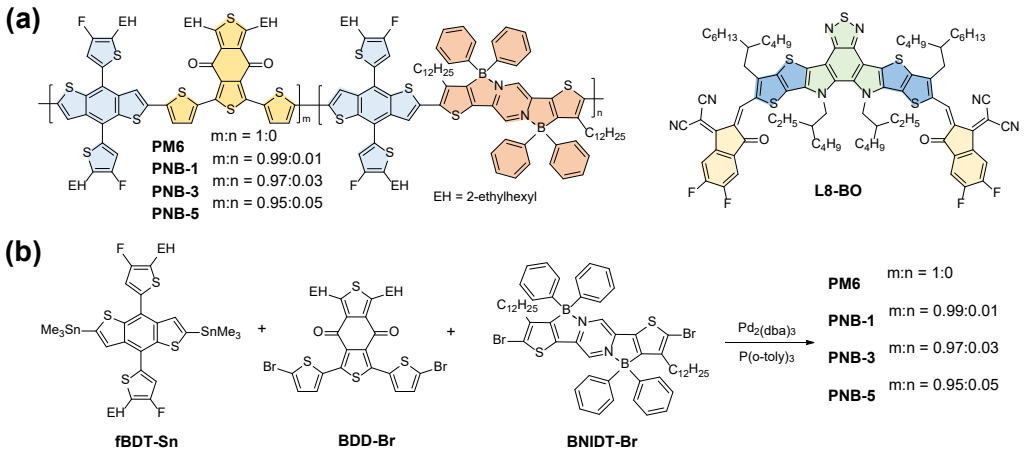

Scheme 1. a) The chemical structures of the terpolymer donors and L8-BO acceptor. b) The synthetic procedures of the terpolymers.

2. Results and Discussion

2.1. Materials Synthesis and Characterization

The synthetic routes of the terpolymers are shown in in **Figure 1b**. Stille-coupling polymerization of organotin monomer (fBDT-Sn) with brominated monomers of BDDBr and BNIDT-Br offered the target random terpolymers, namely PNB-1 (m:n = 0.99:0.01), PNB-3 (m:n = 0.97:0.03) and PNB-5 (m:n = 0.97:0.03), respectively, by varying the feed ratio (m:n) of BDD-Br/BNIDT-Br. The synthetic details are provided in Supporting Information. High temperature gel permeation chromatography was used to estimate their molecular weights, the number average molecular weights (M_n) were estimated to be 49.8, 34.3, and 39.2 kDa, with the corresponding polydispersity index ($Đ$) of 1.76, 1.69, and 1.94 for PNB-1, PNB-3, and PNB-5, respectively. Thermogravimetric analysis (TGA) confirmed their high thermal stability with a decomposition temperature (T_d, 5 % weight loss) over 400 ˚C (**Figure S1**).

2.2 Optical Properties and Energy Levels

The photon absorption properties of these polymers were monitored using UV-vis-NIR absorption spectroscopy. **Figure S2** shows the absorption profiles of these terpolymers in chloroform (CF) solution, which are quite similar to that of PM6 in the wavelength range of 300–650 nm with a comparable high maximum molar extinction coefficient (ε) around 7×10^4

M^{-1} cm^{-1}. With increasing BNIDT unit in the polymer main chain, the resultant terpolymers show a gradually increased absorption in the wavelength range of 650 – 800 nm. This phenomenon is also observed in the related polymer films (**Figure 1a**), the optical bandgaps were estimated to be 1.81, 1.75, 1.67, and 1.57 eV for PM6, PNB-1, PNB-3 and PNB-5, respectively. The enhanced absorption in the range of 650–800 nm properly compensate the weak area between the donors and L8-BO acceptor, which is beneficial for improving the charge generation in the resultant devices.

Figure 1b shows the cyclic voltammetry (CV) curves of the random terpolymers. PM6 was also measured for comparison. The HOMO and lowest unoccupied molecular orbital (LUMO) energy levels of PM6 were estimated to be −5.43 and −3.41 eV, respectively. The introduction of BNIDT block into the PM6 polymer main chain resulted in the deepened HOMO/LUMO energy levels, which were −5.45/−3.44, −5.46/−3.46 and −5.48/−3.49 eV for PNB-1, PNB-3 and PNB-5, respectively. The introduction of BNIDT block effect on the frontier energy levels was also studied by theoretical simulations based on the density functional theory (DFT). **Figure S3** shows the frontier orbitals of BDD and BNIDT blocks (the long alkyl chains were replaced with methyl groups to simplify the calculations). BNIDT shows deeper HOMO/LUMO levels than those of BDD (−5.80/−3.02 eV versus −5.45/−2.16 eV). Therefore, it is expected that the replacement of BDD with BNIDT in the polymer main chain will lower the frontier energy levels. As shown in **Figure 1d**, the HOMO/LUMO for the dimers of PM6, PNB-50 (BDD:BNIDT = 1:1) and PNB-100 (BDD:BNIDT = 0:1) were calculated to be −4.99/−2.62, −5.07/−3.06 and −5.19/−3.14 eV, respectively, which agreed well with the variation trend observed in CV measurements. The deepened HOMO levels would have potential to increase the V_{oc} of the resultant OSCs. Moreover, compared to the more delocalized frontier orbitals of PM6, the BNIDT containing polymers exhibit more separated frontier energy levels with HOMO and LUMO mainly located on the donor and acceptor blocks, respectively. The separated frontier energy levels are expected to reduce the ΔE_{ST} for improving

the ISC of singlet excitons to triplet excitons,[38] and thus the longer lifetime of triplet excitons is favorable for more efficient charge separation.

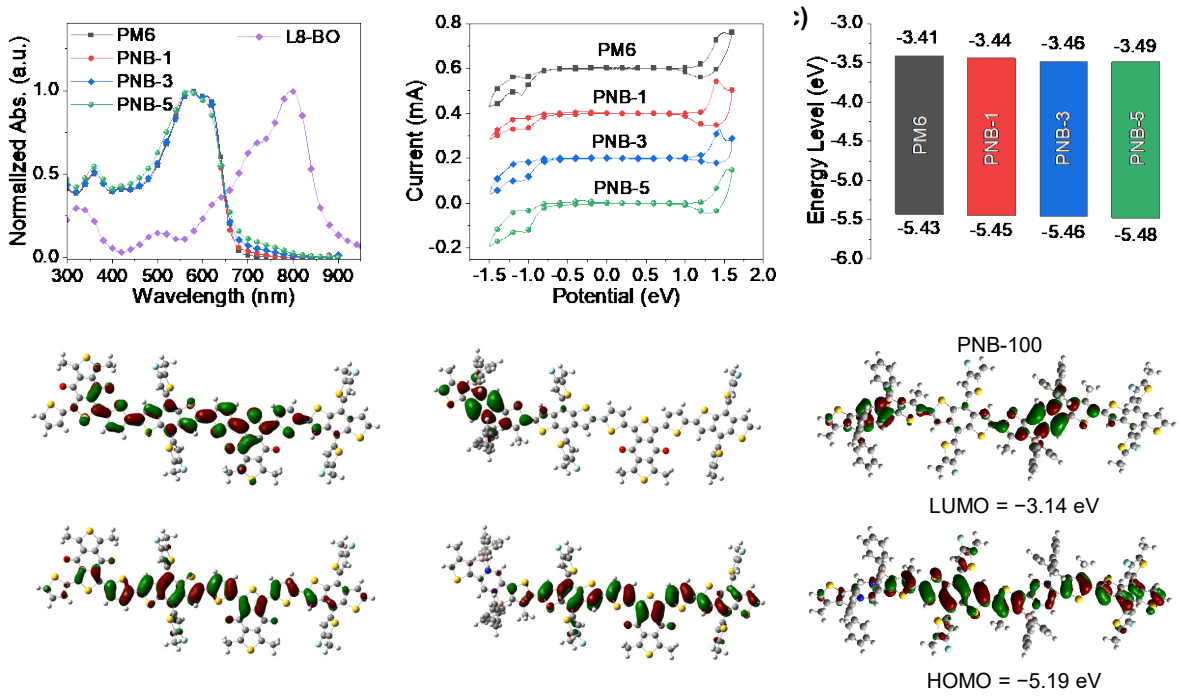

Figure 1. a) Normalized UV-vis-NIR absorption spectra of the polymers and L8-BO. b) CV curves of the polymer films. c) The energy level diagram of the polymers. d) Optimized geometries with frontier orbitals of PM6, PBN-50, and PNB-100 dimers.

2.3. Photovoltaic Properties and Energy Loss

To investigate the photovoltaic properties of these polymer donors, conventional bulk-heterojunction OSCs using L8-BO as the acceptor were fabricated and evaluated. The fabrication and characterization details are presented in Supporting Information. **Figure 2a** shows the current-density (*J*-*V*) curves of the OSCs, and **Table 1** shows the corresponding photovoltaic parameters. The control PM6:L8-BO devices exhibited a high V_{oc} of 0.893 V, a J_{sc} of 25.73 mA cm^{-2} and an FF of 78.00%, delivering a PCE of 17.92%. Using PNB-1:L8-BO as the active layer, the V_{oc} and J_{sc} were increased to 0.903 V and 26.21 mA cm^{-2} with an almost unchanged FF of 78.04%, resulting in a higher PCE of 18.47%. Moreover, a much higher PCE of 19.02% was finally realized in the PNB-3:L8-BO-based devices, owing to the coinstantaneous enhanced V_{oc} of 0.907 V, J_{sc} of 26.59 mA cm^{-2} and FF of 78.86%. To our best

knowledge, this is the best record for the binary blend OSCs using random terpolymers as the electron donors (**Table S1**). For the PNB-5:L8-BO-based devices, the V_{oc} was further elevated to 0.914 V, while the J_{sc} and FF decreased to 25.53 mA cm^{-2} and 76.20%, generating a lower PCE of 17.78%. The gradually increased V_{oc} can be attributed to the progressively deepened HOMO levels of these random terpolymers compared to that of PM6. The largely increased J_{sc} and FF in PNB-3:L8-BO-based devices were mainly originated from the improved charge generation/extraction progresses. The improved device performance was further confirmed by external quantum efficiency (EQE) measurements (**Figure 2b**). PNB-1 and PNB-3-based devices showed consistently higher photo-responses over the given absorption range than that of PM6-based devices, indicating their higher charge extraction. The current density calculated from the EQE integration (J_{EQE}) were 24.92, 25.35 and 25.62 mA cm^{-2} for PM6, PNB-1 and PNB-3 devices, respectively. In contrast, the J_{EQE} was lowered to be 24.74 mA cm^{-2} for PNB-5-based devices, implying their increased charge recombination.

The E_{loss} analysis was conducted to investigate the charge recombination of the OSCs based on these random terpolymers (**Figure 2c-f** and **Table S2**). The E_{loss} can be divided into three contributions: (1) radiative recombination from the absorption above the bandgap ($\Delta E_1 = E_g - qV_{oc,SQ}$), (2) additional radiative recombination from the absorption below the bandgap ($\Delta E_2 = qV_{oc,SQ} - qV_{oc;Rad}$), and (3) non-radiative recombination loss ($\Delta E_3 = kT\ln(EQE_{EL}^{-1})$).[27-28] The bandgaps ($E_g$s) of the blend films were determined from the intersections of electroluminescence and absorption spectra, which were 1.440 eV for PM6, PNB-1, and PNB-3-based blend films, and 1.445 eV for PNB-5-based blend films. Therefore, a moderate small E_{loss} of 0.547 eV was obtained for PM6-based devices. Compared with PM6, the E_{loss} was lowered to 0.537, 0.533, and 0.531 eV for PNB-1, PNB-3, and PNB-5-based devices, respectively. The $V_{oc,SQ}$ were estimated to be 1.173 eV for PM6, PNB-1, and PNB-3-based blend films, and 1.178 eV for PNB-5-based blend films. Therefore, a same ΔE_1 of 0.267 eV was obtained for all these OSCs, which is an avoidable radiative loss. These results

demonstrated the terpolymer had minimal effect on the ΔE_1. The $V_{oc,rad}$ values were 1.105, 1.106, 1.106 and 1.112 eV for PM6, PNB-1, PNB-3 and PNB-5 based OSCs, corresponding to their ΔE_2 of 0.068, 0.067, 0.067 and 0.066 eV, respectively. As could be seen, the additional recombination loss ΔE_2 was already very low in the PM6 based devices, and it was difficult to be further suppressed notably by molecular design. In contrast, PM6-based devices suffered from a relatively high ΔE_3 of 0.212 eV. Fortunately, the ΔE_3 was progressively lowered to 0.203, 0.199 and 0.198 eV for PNB-1, PNB-3 and PNB-5 devices. To our best knowledge, this is hardly any binary blend OSCs possess a low ΔE_3 below 0.2 eV and high PCE over 19%. Therefore, rational design of terpolymers is a promising way to further lower the non-radiative recombination loss for high-performance OSCs.

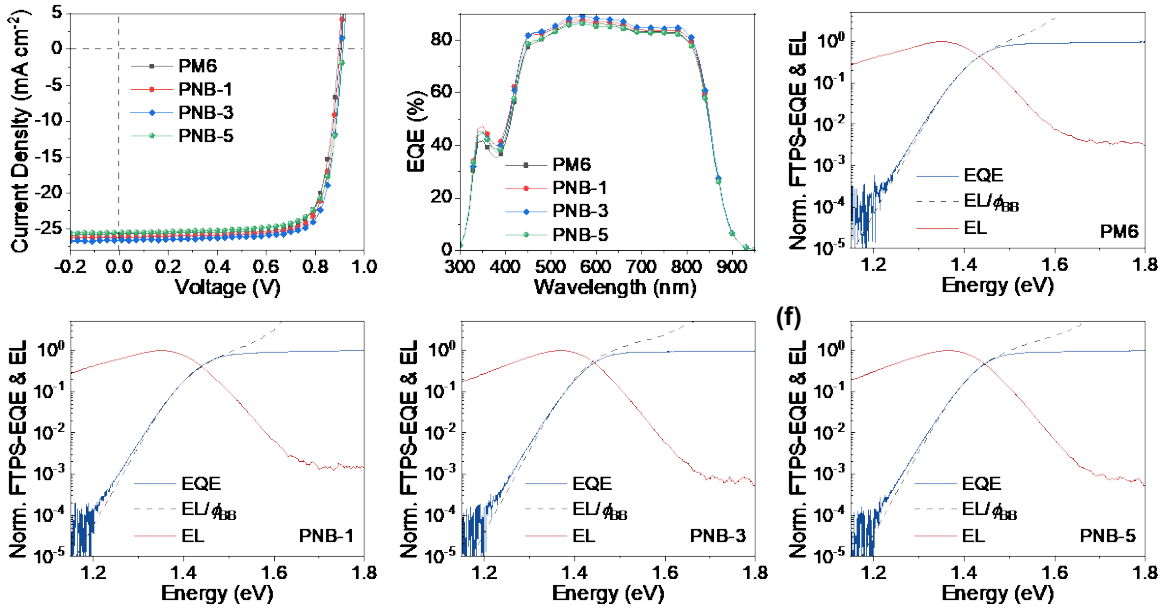

Figure 2. a) *J-V* curves of the OSCs. b) EQE spectra of the OSCs. Normalized FTOS-EQE and EL spectra of the OSCs based on various donors: c) PM6, d) PNB-1, e) PNB-3 and f) PNB-5.

Table 1. Photovoltaic parameters of the various type OSCs.

Active layer	V_{oc} [V]	J_{sc} [mA cm^{-2}]	J_{EQE} [mA cm^{-2}]	FF [%]	PCE [%]
PM6:L8-BO	0.893	25.73	24.92	78.00	17.92

	(0.887±0.003)	(25.66±0.14)		(76.92±0.79)	(17.52±0.20)
PNB-1:L8-BO	0.903	26.21	25.35	78.04	18.47
	(0.899±0.004)	(26.14±0.17)		(77.33±0.54)	(18.17±0.16)
PNB-3:L8-BO	0.907	26.59	25.62	78.86	19.02
	(0.902±0.003)	(26.46±0.16)		(78.37±0.55)	(18.67±0.22)
PNB-5:L8-BO	0.914	25.53	24.74	76.20	17.78
	(0.910±0.004)	(25.36±0.12)		(75.48±0.66)	(17.41±0.19)

[a)]The average values with standard deviations in parentheses were calculated from at least 10 individual devices.

2.4. Charge Transfer and Recombination Mechanisms

The photoluminescence (PL) emission spectra of the polymers were measured to disclose the effect of B-N bond on the charge transfer and recombination of the OSCs (**Figure 3a-c**). The fluorescent emission peaks of these terpolymers located at around 667 nm, corresponding to the E_{S1} of 1.86 eV. In addition, the phosphorescent emission peaks located at 753, 781 and 781 nm for PNB-1, PNB-3 and PNB-5, corresponding to their E_{T1} values of 1.65, 1.59, and 1.59 eV, respectively. Therefore, the quite small ΔE_{ST} values were estimated to be 0.21, 0.27 and 0.27 eV for PNB-1, PNB-3 and PNB-5, respectively. The small ΔE_{ST} is favorable for electronic coupling of S_1 and T_1, and thus promoting the ISC of excitons from S_1 to T_1. PM6 showed a fluorescent emission at 680 nm, corresponding to an E_{S1} of 1.82 eV (**Figure 3d**). Unfortunately, the phosphorescent emission of PM6 was hardly detected, which was due to its large ΔE_{ST} (≈ 0.7 eV for organic semiconductors), blocking energetically the ISC process from S_1 to T_1 (**Figure 3e**). The E_{CT} of PM6 device is 1.37 eV ($E_g - \Delta E_2$), corresponding to a ΔE_{CT} of 0.45 eV. In this sense, non-radiative recombination *via* triplet state could contribute the major terminal loss channel of photocurrent. In comparison, the ΔE_{ST} values of the terpolymers are much smaller than their ΔE_{CT} (0.48–0.49 eV) values, which means their T_1 states are above their CT states, thus preventing the non-radiative recombination *via* triplet states (**Figure 3f**). In this case, triplet excitons with inherently longer lifetimes also benefit the charge separation in these

terpolymer-based devices. Although PNB-5 possessed a very low ΔE_{ST}, the device performance was even smaller than PM6-based devices. This reduced device performance was caused by the unfavorable morphology of PNB-5:L8-BO blend, which could also induced severe non-radiative recombination.

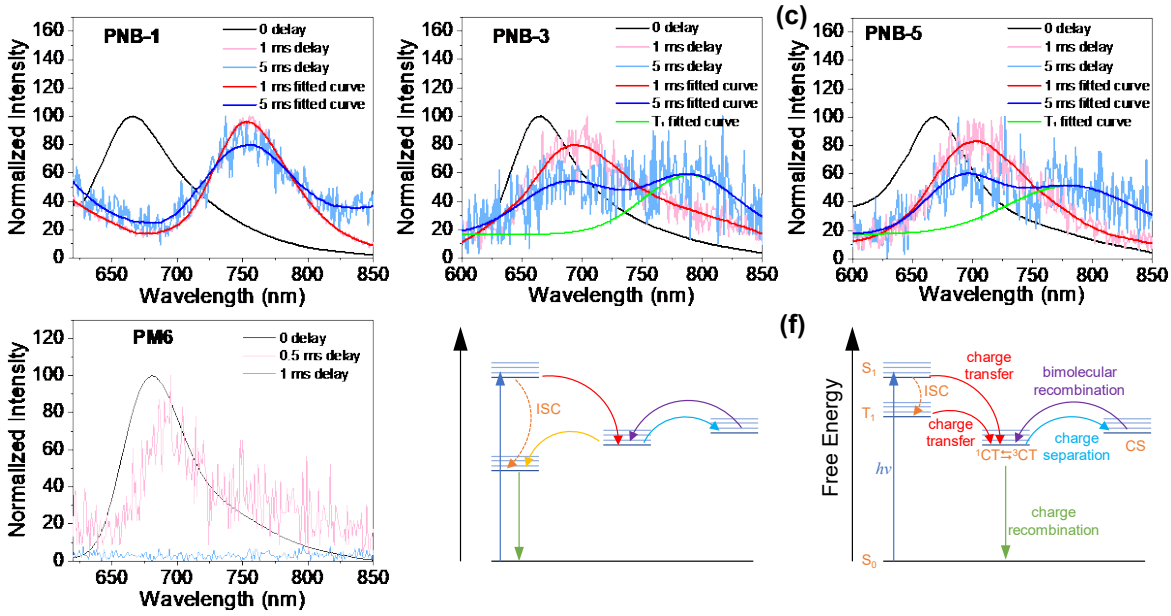

Figure 3. PL emission spectra of the polymer films at 77 K with different delay time: a) PNB-1, b) PNB-3, c) PNB-5 and d) PM6. The Jablonski diagram of the electronic states in the polymers: e) T_1 state below the CT state and f) T_1 state above the CT state.

2.5. Morphology Properties and Charge Carrier Mobilities

Grazing incidence wide angle X-ray scattering (GIWAXS) measurements were performed to study the molecular packing behaviors (**Figure 4**). PM6 showed (100) diffraction in both the in-plane and out-of-plane directions, indicating the coexist face-on and edge-on packing of PM6 film. The lamellar stacking distance (d_L) was calculated to be 2.10 nm based on the (100) peak at $q_{xy} = 2.99$ nm^{-1}. The (010) diffraction appeared mainly in the out-of-plane direction, showing the more preferred face-on packing. The (010) peak located at $q_z = 17.3$ nm^{-1}, corresponding to the π-π stacking distance (d_π) of 0.362 nm. If introducing a small amount (within 5%) of NBIDT block, there was minimal effect on the molecular packing behaviors of these terpolymers, and the d_L was increased slightly to 2.17 nm for all three terpolymers (**Figure S4**).

The (010) peak showed mildly decreased intensity and increased d_{π} of 0.363 nm for PNB-1, 0.365 nm for PNB-3 and 0.366 nm for PNB-5, respectively. The slightly increased d_L and d_{π} were due to the bulky benzene ring in BNIDT block with a large steric hindrance, which hampered the molecular stacking. In the active blends, the integral area of the (100) peak ($A_{(100)}$) was decreased gradually for those polymers with increasing the BNIDT amount, while its coherent length ($CCL_{(100)}$) was found to be mildly changed (**Figure 4k**). The results suggested that the gradually lowered molecular packing of these polymers in the related active blends. By comparison, the integral area of the (11-1) peak ($A_{(11\text{-}1)}$) for L8-BO was increased first and then decreased, while its coherent length ($CCL_{(11\text{-}1)}$) was notably increased (**Figure 4k**). Among them, PNB-3:L8-BO film exhibited relatively high and balanced peak intensity as well as CCL for both the polymer and acceptor, which would be beneficial for hole and electron transport at the same time. In contrast, PNB-3:L8-BO had the highest CCL but relatively low peak intensity for both polymer donor and acceptor, which implied that the inhomogeneous molecular packing affected the corresponding charge transport property.

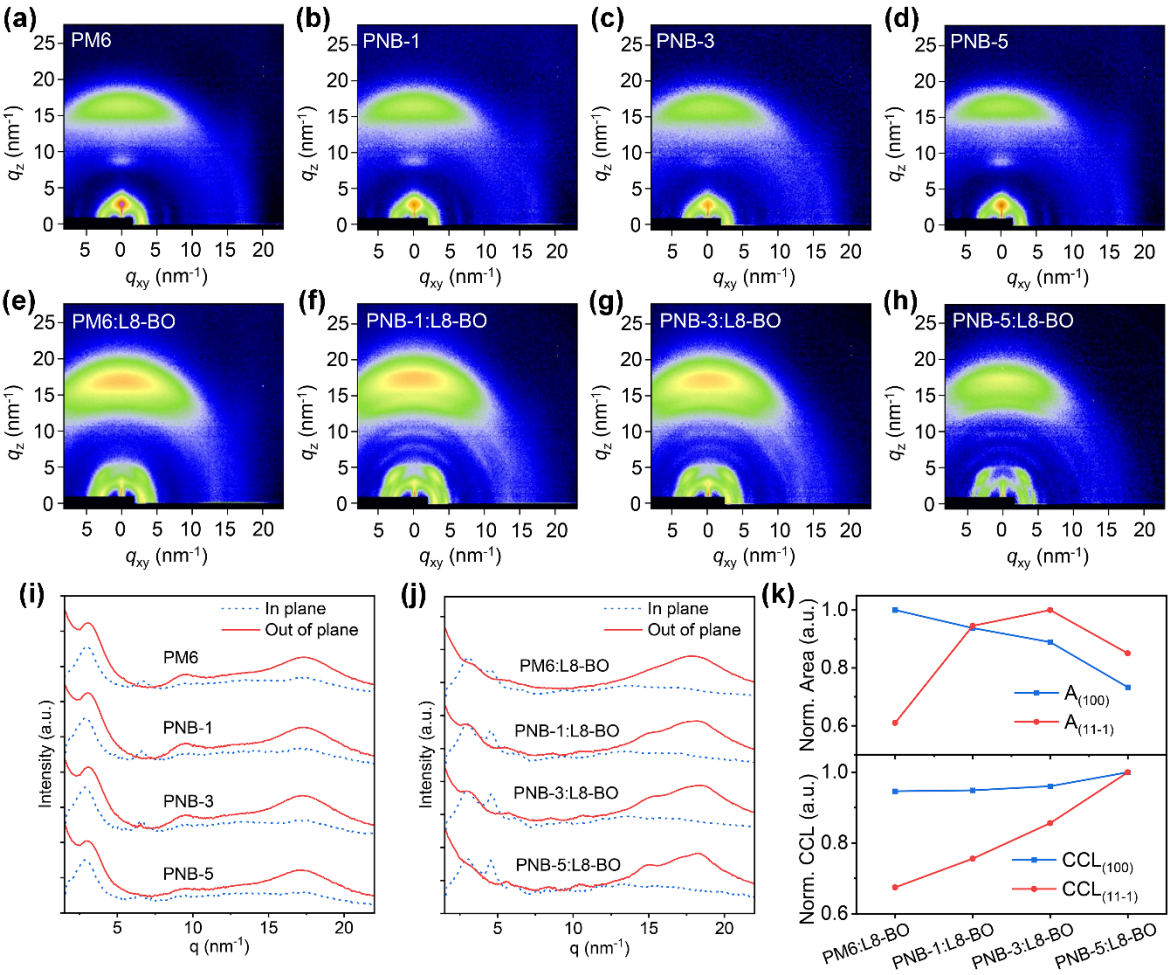

Figure 4. a-h) GIWAXS patterns of the pristine and blend films. i-j) The in-plane and out-of-plane line-cuts for the (i) pristine and (j) blend films. k) The normalized peak area and CCL for the (100) peaks of the donors and (11-1) peaks of the acceptor.

Space-charge-limited current (SCLC) method was used to study the charge transport properties (**Figure S5** and **Table S3**). The hole/electron mobilities (μ_h/μ_e) of the PM6:L8-BO, PNB-1:L8-BO, PNB-3:L8-BO and PNB-5:L8-BO blends were $4.1\times10^{-4}/3.0\times10^{-4}$, $4.8\times10^{-4}/3.6\times10^{-4}$, $4.5\times10^{-4}/4.0\times10^{-4}$ and $2.2\times10^{-4}/3.4\times10^{-4}$ cm^2 V^{-1} s^{-1}, which corresponded to the μ_h/μ_e ratios of 1.4, 1.3, 1.1 and 0.65, respectively. The PNB-3:L8-BO exhibited relatively high and balanced charge transport, which enabled to suppress the charge accumulation and recombination. By contrast, PNB-5:L8-BO showed the lowest and unbalanced charge carrier mobilities, which could accelerate the non-radiative recombination and lower the device performance of the related OSCs.

Atomic force microscopy (AFM) measurements were conducted to further study the morphology properties of these active blends (**Figure 5**). PM6:L8-BO exhibited a rather smooth top surface with a small root-mean-square roughness (R_q) of 0.98 nm. Well-defined nanofibrils could be observed from its tapping phase image, which was conducive to the charge separation and transport. With increasing the BNIDT ratio in the terpolymers, the corresponding active blends exhibited continuously increased R_q of 1.26 nm for PNB-1:L8-BO, 1.74 nm for PNB-3:L8-BO, and 2.15 nm for PNB-5:L8-BO blends, respectively, indicating the strengthened phase separation step by step. The nanofibrils became much wider with increasing the BNIDT ratio in the terpolymers, and PNB-3:L8-BO showed the optimized phase separation with appropriate fibril networks, which was answerable for its more efficient charge transport and higher FF. Nevertheless, PNB-5:L8-BO showed a more inhomogeneous phase separation with relatively large aggregates in the active blend, which acted as trap sites for inducing sever non-radiative recombination and lowering the device performances. Therefore, in addition to lower the ΔE_{ST}, rational control the morphology is also of great importance to suppress the non-radiative recombination for higher device performance.

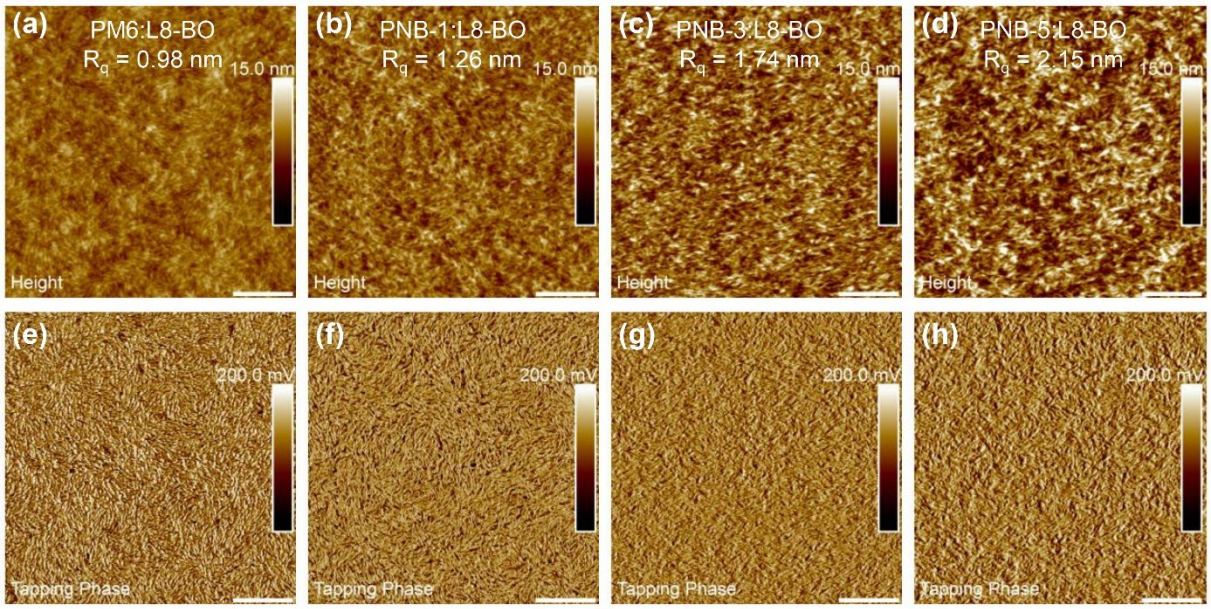

Figure 5. AFM height and tapping phase images of various active blends. a,e) PM6:L8-BO. b,f) PNB-1:L8-BO. c,g) PNB-3:L8-BO. d,h) PNB-5:L8-BO.

2.6. Charge Transfer and Recombination Kinetics

To further clarify the charge transfer and recombination kinetics, femtosecond transient absorption spectroscopy (fs-TAS) measurements were performed. **Figure S6** shows the ground-state bleach (GSB) signals of PM6 and PNB-3 in the range of 550–650 nm, and **Figure 6a** shows the GSB of L8-BO around 600–800 nm. The GSB signals of PNB-3 at 630 nm exhibit slower decay than that of PM6, which indicates its longer exciton lifetime (**Figure 6d**). The longer exciton lifetime is expected to not only improve the exciton diffusion length but also contribute higher exciton dissociation efficiency in the blend films.[39] The fs-TAS of the PM6:L8-BO and PNB-3:L8-BO are shown in **Figure 6b-c.** The TA kinetics of L8-BO polaron state can be extracted from the pristine L8-BO film and the blend films (**Figure 6e**). The PNB-3:L8-BO blend film shows slower decay of the polaron state at 820 nm, suggesting that the improved morphology suppresses non-radiative recombination.[14] The kinetics at 560 nm in two blends are extracted and fitted with a double exponential decay function (**Figure 6f**). The PNB-3:L8-BO blend exhibited the faster (a smaller τ_1 of 0.65 *vs* 0.89 ps) and more efficient hole transfer compared to PM6:L8-BO. Therefore, the improved hole transfer and suppressed non-radiative recombination were answerable for the higher device performance of PNB-3 devices.

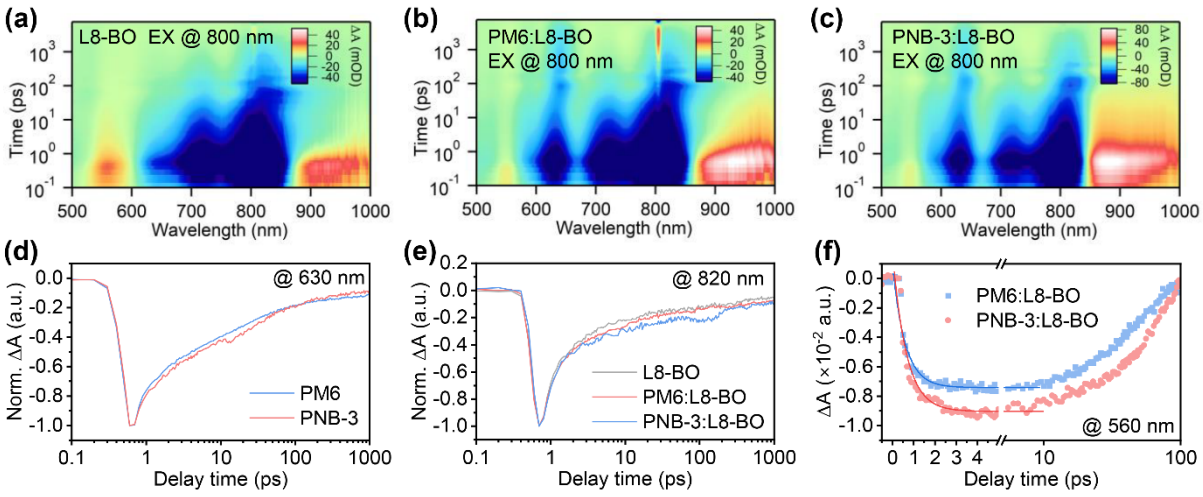

Figure 6. Color plots of fs-TAS of various films: a) L8-BO, b) PM6:L8-BO, c) PNB-3:L8-BO. d) Kinetics of the GSB signals of the pristine polymers at 630 nm. e) Kinetics of the polaron state of L8-BO and the blend films at 820 nm. f) kinetics of the GSB signals of the blend films at 560 nm.

3. Conclusions

In this work, we report the design and synthesis of a series of WBG triplet polymers, namely PNB-1, PNB-3 and PNB-5, for high-performance OSC applications. By introducing a BNIDT block into the PM6 polymer main chain, its higher electron affinity resulted in the deepened HOMOs, and the opposite resonance effect of B-N bond led to a smaller ΔE_{ST} (0.2–0.3 eV) than the ΔE_{CT} (0.48–0.49 eV) of the corresponding random terpolymers. The introduction of BNIDT block was also conducive to optimize the morphology of the active blend films. Therefore, the random terpolymers-based devices achieved the higher V_{oc}, and non-radiative recombination *via* the terminal triplet loss channels and morphology traps was effectively suppressed. The PNB-3:L8-BO exhibited both small ΔE_{ST} and optimized morphology, favoring the more efficient charge transfer and transport. As a result, the simultaneously enhanced V_{oc} of 0.907 V, J_{sc} of 26.59 mA cm^{-2} and FF of 78.86% contributed to the champion PCE of 19.02%. Our results indicate that the introduction of B-N bond into the benchmark polymers is a possible avenue toward high-performance of OSCs with further lowered non-radiative loss.

Supporting Information

Supporting Information is available from the Wiley Online Library or from the author.

Acknowledgements

This work was financially supported by the National Natural Science Foundation of China (NSFC, 21825502, 22075190, 21905185 and 22105135), the School Local Science and Technology Cooperation Special Funds of Sichuan University Zigong City (2020CDYB-28), Special Fund for Strategic Cooperation Between Sichuan University and Yibin Municipal People's Government (2020CDZG-6) and the Fundamental Research Funds for the Central Universities (YJ201957, YJ202069 and YJ202116). The authors also thank National

Synchrotron Light Source II (NSLS-II, Contract No. DE-SC0012704) Brookhaven National Laboratory for providing GIWAXS experiment time.

Received: ((will be filled in by the editorial staff))

Revised: ((will be filled in by the editorial staff))

Published online: ((will be filled in by the editorial staff))

References

[1] G. Zhang, F. R. Lin, F. Qi, T. Heumuller, A. Distler, H. J. Egelhaaf, N. Li, P. C. Y. Chow, C. J. Brabec, A. K. Jen, H. L. Yip, *Chem. Rev.* **2022**, *122*, 14180.

[2] J. Wang, P. Xue, Y. Jiang, Y. Huo, X. Zhan, *Nat. Rev. Chem.* **2022**, *6*, 614.

[3] Y. D. Zhang, Y. T. Ji, Y. Y. Zhang, W. Q. Zhang, H. L. Bai, M. Z. Du, H. Wu, Q. Guo, E. J. Zhou, *Adv. Funct. Mater.* **2022**, *32*, 2205115.

[4] Y. Z. Lin, J. Y. Wang, Z. G. Zhang, H. T. Bai, Y. F. Li, D. B. Zhu, X. W. Zhan, *Adv. Mater.* **2015**, *27*, 1170.

[5] J. Yuan, Y. Q. Zhang, L. Y. Zhou, G. C. Zhang, H. L. Yip, T. K. Lau, X. H. Lu, C. Zhu, H. J. Peng, P. A. Johnson, M. Leclerc, Y. Cao, J. Ulanski, Y. F. Li, Y. P. Zou, *Joule* **2019**, *3*, 1140.

[6] Z. Luo, R. Ma, J. Yu, H. Liu, T. Liu, F. Ni, J. Hu, Y. Zou, A. Zeng, C. J. Su, U. S. Jeng, X. Lu, F. Gao, C. Yang, H. Yan, *Natl. Sci. Rev.* **2022**, *9*, nwac076.

[7] Z. Luo, Y. Gao, H. Lai, Y. Li, Z. Wu, Z. Chen, R. Sun, J. Ren, C. e. Zhang, F. He, H. Woo, J. Min, C. Yang, *Energy Environ. Sci.* **2022**, *15*, 4601.

[8] X. Xu, T. Yu, Z. Bi, W. Ma, Y. Li, Q. Peng, *Adv. Mater.* **2018**, *30*, 1703973.

[9] Q. Liu, Y. Jiang, K. Jin, J. Qin, J. Xu, W. Li, J. Xiong, J. Liu, Z. Xiao, K. Sun, S. Yang, X. Zhang, L. Ding, *Sci. Bull.* **2020**, *65*, 272.

[10] J. Wang, Y. Cui, Y. Xu, K. Xian, P. Bi, Z. Chen, K. Zhou, L. Ma, T. Zhang, Y. Yang, Y. Zu, H. Yao, X. Hao, L. Ye, J. Hou, *Adv. Mater.* **2022**, *34*, 2205009.

[11] Y. Cui, Y. Xu, H. Yao, P. Bi, L. Hong, J. Zhang, Y. Zu, T. Zhang, J. Qin, J. Ren, Z. Chen, C. He, X. Hao, Z. Wei, J. Hou, *Adv. Mater.* **2021**, *33*, 2102420.

[12] X. Xu, G. Zhang, L. Yu, R. Li, Q. Peng, *Adv. Mater.* **2019**, *31*, 1906045.

[13] X. Xu, Y. Li, Q. Peng, *Adv. Mater.* **2022**, *34*, 2107476.

[14] L. Zhu, M. Zhang, J. Xu, C. Li, J. Yan, G. Zhou, W. Zhong, T. Hao, J. Song, X. Xue, Z. Zhou, R. Zeng, H. Zhu, C. C. Chen, R. C. I. MacKenzie, Y. Zou, J. Nelson, Y. Zhang, Y. Sun, F. Liu, *Nat. Mater.* **2022**, *21*, 656.

[15] X. Xu, L. Yu, H. Meng, L. Dai, H. Yan, R. Li, Q. Peng, *Adv. Funct. Mater.* **2022**, *32*, 2108797.

[16] Z. Zheng, J. Wang, P. Bi, J. Ren, Y. Wang, Y. Yang, X. Liu, S. Zhang, J. Hou, *Joule* **2022**, *6*, 171.

[17] M. Zhou, C. Liao, Y. Duan, X. Xu, L. Yu, R. Li, Q. Peng, *Adv. Mater.* **2022**, 10.1002/adma.202208279.

[18] K. Chong, X. Xu, H. Meng, J. Xue, L. Yu, W. Ma, Q. Peng, *Adv. Mater.* **2022**, *34*, 2109516.

[19] K. Jiang, J. Zhang, C. Zhong, F. R. Lin, F. Qi, Q. Li, Z. X. Peng, W. Kaminsky, S. H. Jang, J. W. Yu, X. Deng, H. W. Hu, D. Shen, F. Gao, H. Ade, M. Xiao, C. F. Zhang, A. K. Y. Jen, *Nat. Energy* **2022**, *7*, 1076.

[20] W. Gao, F. Qi, Z. Peng, F. R. Lin, K. Jiang, C. Zhong, W. Kaminsky, Z. Guan, C. S. Lee, T. J. Marks, H. Ade, A. K. Y. Jen, *Adv. Mater.* **2022**, *34*, 2202089.

[21] C. He, Y. Pan, Y. Ouyang, Q. Shen, Y. Gao, K. Yan, J. Fang, Y. Chen, C.-Q. Ma, J. Min, C. Zhang, L. Zuo, H. Chen, *Energy Environ. Sci.* **2022**, *15*, 2537.

[22] D. Li, N. Deng, Y. Fu, C. Guo, B. Zhou, L. Wang, J. Zhou, D. Liu, W. Li, K. Wang, Y. Sun, T. Wang, *Adv. Mater.* **2022**, 10.1002/adma.202208211, e2208211.

[23] R. Sun, Y. Wu, X. Yang, Y. Gao, Z. Chen, K. Li, J. Qiao, T. Wang, J. Guo, C. Liu, X. Hao, H. Zhu, J. Min, *Adv. Mater.* **2022**, *34*, 2110147.

[24] Y. Wei, Z. Chen, G. Lu, N. Yu, C. Li, J. Gao, X. Gu, X. Hao, G. Lu, Z. Tang, J. Zhang, Z. Wei, X. Zhang, H. Huang, *Adv. Mater.* **2022**, *34*, 2204718.

[25] L. Zhan, S. Li, Y. Li, R. Sun, J. Min, Y. Chen, J. Fang, C. Q. Ma, G. Zhou, H. Zhu, L. Zuo, H. Qiu, S. Yin, H. Chen, *Adv. Energy Mater.* **2022**, *12*, 2201076.

[26] N. A. Ran, J. A. Love, M. C. Heiber, X. Jiao, M. P. Hughes, A. Karki, M. Wang, V. V. Brus, H. Wang, D. Neher, H. Ade, G. C. Bazan, T. Q. Nguyen, *Adv. Energy Mater.* **2018**, *8*, 1701073.

[27] S. Liu, J. Yuan, W. Y. Deng, M. Luo, Y. Xie, Q. B. Liang, Y. P. Zou, Z. C. He, H. B. Wu, Y. Cao, *Nat. Photonics* **2020**, *14*, 300.

[28] J. Liu, S. S. Chen, D. P. Qian, B. Gautam, G. F. Yang, J. B. Zhao, J. Bergqvist, F. L. Zhang, W. Ma, H. Ade, O. Inganas, K. Gundogdu, F. Gao, H. Yan, *Nat. Energy* **2016**, *1*, 16089.

[29] X. N. Zhang, C. Li, J. Q. Xu, R. Wang, J. L. Song, H. Zhang, Y. X. Li, Y. N. Jing, S. L. Li, G. B. Wu, J. Zhou, X. Li, Y. Y. Zhang, X. Li, J. Q. Zhang, C. F. Zhang, H. Q. Zhou, Y. M. Sun, Y. Zhang, *Joule* **2022**, *6*, 444.

[30] F. Huang, T. He, M. Li, L. Meng, W. Feng, H. Liang, Y. Zhou, X. Wan, C. Li, G. Long, Z. Yao, Y. Chen, *Chem. Mater.* **2022**, *34*, 6009.

[31] J. Song, L. Zhu, C. Li, J. Xu, H. Wu, X. Zhang, Y. Zhang, Z. Tang, F. Liu, Y. Sun, *Matter* **2021**, *4*, 2542.

[32] C. Li, J. Zhou, J. Song, J. Xu, H. Zhang, X. Zhang, J. Guo, L. Zhu, D. Wei, G. Han, J. Min, Y. Zhang, Z. Xie, Y. Yi, H. Yan, F. Gao, F. Liu, Y. Sun, *Nat. Energy* **2021**, *6*, 605.

[33] S. M. Menke, N. A. Ran, G. C. Bazan, R. H. Friend, *Joule* **2018**, *2*, 25.

[34] G. Han, T. Hu, Y. Yi, *Adv. Mater.* **2020**, *32*, 2000975.

[35] J. Benduhn, K. Tvingstedt, F. Piersimoni, S. Ullbrich, Y. Fan, M. Tropiano, K. A. McGarry, O. Zeika, M. K. Riede, C. J. Douglas, S. Barlow, S. R. Marder, D. Neher, D. Spoltore, K. Vandewal, *Nat. Energy* **2017**, *2*, 17053.

[36] Z. Chen, X. Chen, Z. Jia, G. Zhou, J. Xu, Y. Wu, X. Xia, X. Li, X. Zhang, C. Deng, Y. Zhang, X. Lu, W. Liu, C. Zhang, Y. Yang, H. Zhu, *Joule* **2021**, *5*, 1832.

[37] G. Han, Y. Yi, *Acc. Chem. Res.* **2022**, *55*, 869.

[38] S. Pang, Z. Wang, X. Yuan, L. Pan, W. Deng, H. Tang, H. Wu, S. Chen, C. Duan, F. Huang, Y. Cao, *Angew. Chem. Int. Ed.* **2021**, *60*, 8813.

[39] L. Zhou, L. Meng, J. Zhang, C. Zhu, S. Qin, I. Angunawela, Y. Wan, H. Ade, Y. Li, *Adv. Funct. Mater.* **2021**, *32*, 2109271.

A series of random terpolymers were developed by introducing the B-N bond into the polymer chain of PM6, which enabled to the lower HOMO level, reduce the ΔE_{ST} and optimize the morphology of the active blend, thus contributing to a high PCE of 19.02% of the devices with reduced E_{loss} and charge recombination.

B. Pang, C. T. Liao, X. P. Xu,* S. Q. Peng, J. L. Xia,* Y. Y. Guo, Y. Xie, Y. T. Chen, C. H. Duan, H. B. Wu,* R. P. Li, and Qiang Peng*

B-N Bond Embedded Triplet Terpolymers with Small Singlet-Triplet Energy Gaps for Suppressing Non-Radiative Recombination and Improving Blend Morphology in Organic Solar Cells

ToC figure (55 mm broad × 50 mm high)

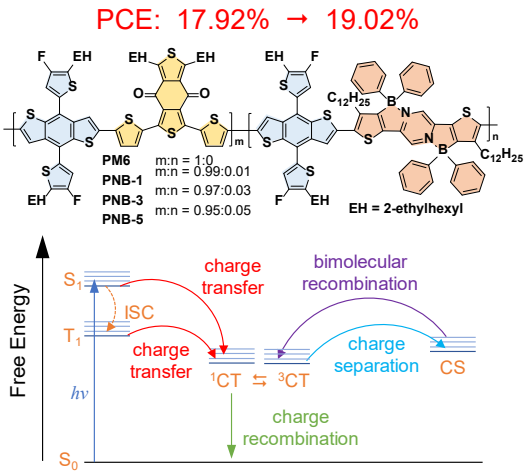

Supporting Information

B-N Bond Embedded Triplet Terpolymers with Small Singlet-Triplet Energy Gaps for Suppressing Non-Radiative Recombination and Improving Blend Morphology in Organic Solar Cells

Bo Pang, Chentong Liao, Xiaopeng Xu, Shaoqian Peng, Jianlong Xia,* Yuanyuan Guo, Yuan Xie, Yuting Chen, Chunhui Duan, Hongbin Wu,* Ruipeng Li, and Qiang Peng**

B. Pang, C. T. Liao, Dr. X. P. Xu, Dr. L. Y. Yu, Prof. Q. Peng
School of Chemical Engineering and State Key Laboratory of Polymer Materials Engineering, Sichuan University, Chengdu 610065, P. R. China. Email: xpxu@scu.edu.cn; qiangpeng@scu.edu.cn

S. Q. Peng, Prof. J. L. Xia
School of Chemistry, Chemical Engineering and Life Science, Wuhan University of Technology, No. 122 Luoshi Road, Wuhan 430070, P. R. China. Email: jlxia@whut.edu.cn

Dr. Y. Y. Guo
Division of Physics and Applied Physics School of Physical and Mathematical Sciences Nanyang Technological University 21 Nanyang Link, Singapore 637371, Singapore.

Prof. C. H. Duan, Y. Xie, Y. T. Chen, Prof. H. B. Wu
Institute of Polymer Optoelectronic Materials and Devices, State Key Laboratory of Luminescent Materials and Devices, South China University of Technology, Guangzhou 510640, P. R. China. Email: hbwu@scut.edu.cn

Dr. R. P. Li
National Synchrotron Light Source II Brookhaven National Lab, Suffolk, Upton, NY 11973, USA.

1. Materials and Methods

Materials: PM6, fBDT-Sn and BDD-Br were purchased Solarmer Materials Inc. L8-BO and PNDIT-F3N were purchased from eflexPV Inc. BNIDT-Br was synthesized according to previous report.[1] All the other chemicals were purchased from Aladdin, Adamas, Sigma-Aldrich, and Alfa Asear Chemical Co., and used without further purification. All solvents were freshly distilled immediately prior to use.

General synthetic procedure of the polymers: fBDT-Sn (0.1 g, 0.1063 mmol) and bromide monomers of BDD-Br and BNIDT-Br at varied ratios (0.99/0.01, 0.97/0.03, 0.95/0.05) were dissolved in toluene (5 mL), $Pd_2(dba)_3$ (1.95 mg, 2% mmol) and P(*o*-tolyl)$_3$ (2.59 mg, 8% mmol) were added to the mixture being flushed with argon for five minutes. Then, the reaction mixtures were purged with argon for another 15 min. The reactions were stirred at 110 °C for 1 h until the reaction mixture becomes viscous. After finished, the reaction mixture was cooled down to room temperature and precipitated into methanol (200 mL). The crude polymer was subjected to Soxhlet extractions with methanol, hexane, and acetone to remove the impurities and oligomers. Then the chloroform fraction was concentrated, and the solution was filtered through a silica gel column. The final solution was concentrated and precipitated in methanol to get a dark solid. The yields are around 70%.

PNB-1: fBDT-Sn (100 mg, 0.1063 mmol), BDD-Br (80.66 mg, 0.1052 mmol), BNIDT-Br (1.13 mg, 1.06 umol). Yield (105 mg, 81%). Elemental analysis calcd (%) for PNB-1 ($C_{67.8}H_{75.86}F_{1.98}B_{0.02}N_{0.02}O_{1.98}S_{7.94}$): N, 0.02%; C, 67.02%; H, 6.29%; S, 20.95%. Found: N, 0.04%; C, 67.32%; H, 6.54%; S, 20.36%.

PNB-3: fBDT-Sn (100 mg, 0.1063 mmol), BDD-Br (79.05 mg, 0.1031 mmol), BNIDT-Br (3.40 mg, 3.19 umol). Yield (110 mg, 86%). Elemental analysis calcd (%) for PNB-3 ($C_{67.4}H_{75.58}F_{1.94}B_{0.06}N_{0.06}O_{1.94}S_{7.82}$): N, 0.07%; C, 67.10%; H, 6.31%; S, 20.78%. Found: N, 0.09%; C, 67.92%; H, 6.67%; S, 20.25%.

PNB-5: fBDT-Sn (100 mg, 0.1063 mmol), BDD-Br (77.43 mg, 0.1010 mmol), DTBT-Br (5.67 mg, 5.32 umol). Yield (98 mg, 77%). Elemental analysis calcd (%) for PNB-5 ($C_{67}H_{75.3}F_{1.9}B_{0.1}N_{0.1}O_{1.9}S_{7.7}$): N, 0.12%; C, 67.26%; H, 6.34%; S, 20.63%. Found: N, 0.17%; C, 68.15%; H, 6.48%; S, 20.12%.

Methods: UV-vis spectra were obtained on a Shimadzu 2700 spectrophotometer. GIWAXS measurements were performed at Complex Materials Scattering (CMS) beamline of the National Synchrotron Light Source II (NSLS-II), Brookhaven National Lab. Droplet contact angle was measured on a Krüss DSA100 contact angle meter. AFM images were obtained by using a Bruker Inova atomic microscope in tapping mode. Femtosecond transient absorption (fs-TA) spectroscopy experiments were performed using a home-built system with a Ti: sapphire regenerative amplified laser system (Coherent Legend Elite). The probe beam was generated by focusing part of the fundamental femtosecond laser beam onto a 3-mm-thick sapphire plate or 4 mm-thick Yttrium aluminum garnet plate for visible (Vis) and near-IR (NIR) spectral windows, respectively. 800 nm laser is used to selectively excite NFAs. TA results in this work are presented in the unit of ΔOD, negative features can reflect ground-state bleaching (GSB) or stimulated emission (SE), a positive signal is an excited-state absorption (ESA). During TA measurements, the samples were kept in nitrogen to avoid photodegradation. The pump fluence was kept at <5 μJ cm^{-2} to minimize the exciton−exciton annihilation effect.

2. Device Fabrication and Measurements

Device fabrication: The patterned indium tin oxide (ITO, sheet resistance = 15 Ω $square^{-1}$) glass substrates were sequentially ultrasonicated with detergent, deionized water, acetone, and isopropanol. Then, the ITO glasses were treated with UV-ozone for 30 min. Poly(3,4-ethylenedioxythiophene):polystyrene sulfonate (PEDOT:PSS) (Bay PVP. Al 4083, Bayer AG) was filtrated through a 0.45 μm nylon filter and then spin-coated on the cleaned ITO substrates at 5000 rpm for 60 s to form a thin layer (35 nm). The polymer:L8-BO solution (1:1.2 by weight and total concentration of 15.4 mg/mL in chloroform with 0.25 v% of diiodomethane additive)

was spin-coated on the ITO/PEDOT:PSS substrates at a speed of 3000 rpm for 30 s to access the active layer with ~100 nm thickness. Then the substrates were put onto a hot plate and annealed at 100 °C for 5 min. PNDIT-F3N solution (0.5 mg/mL in methanol with 5 v% of acetic acid) was spin-coated on the top of the active layer to form a thin cathode interlayer (~10 nm). Finally, argentum electrode (Ag, 100 nm) was deposited under high vacuum (~10^{-5} Pa) in an evaporation chamber. The device area was exactly fixed at 4.00 mm^2.

Device measurements: The *I-V* characterization was performed on a computer-controlled Keithley 2400 Source under AM1.5G (100 mW cm^{-2}) using a solar simulator (XES-70S1, SAN-EI), which was calibrated by a standard Si solar cell (AK-200, Konica Minolta, Inc.). The EQE values were measured with an EQ-R solar quantum efficiency test system (Enlitech Co., Ltd., Taiwan, China). All fabrication and characterization processes, except for the HTLs preparation and EQE measurements, were conducted in a high purity argon filled glove box.

3. Supplementary Figures

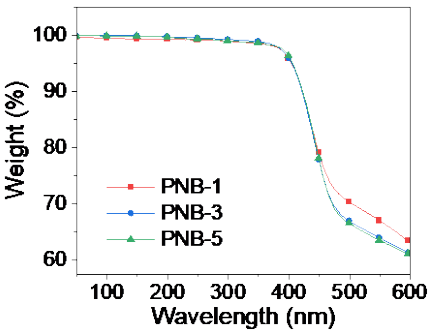

Figure S1. Thermogravimetric analysis (TGA) curves of the terpolymers measured at a heating rate of 10 oC min^{-1} in nitrogen atmosphere.

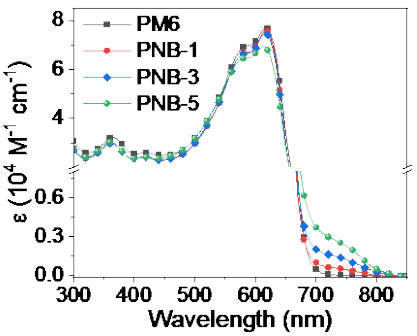

Figure S2. Molar extinction coefficient profiles of the polymers in CF solution.

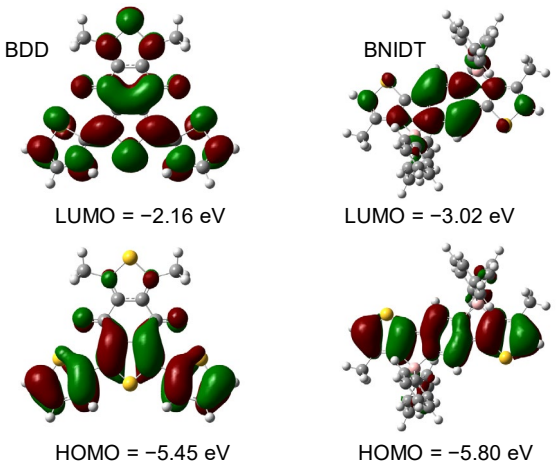

Figure S3. Optimized geometries with frontier orbitals of BDD and BNIDT.

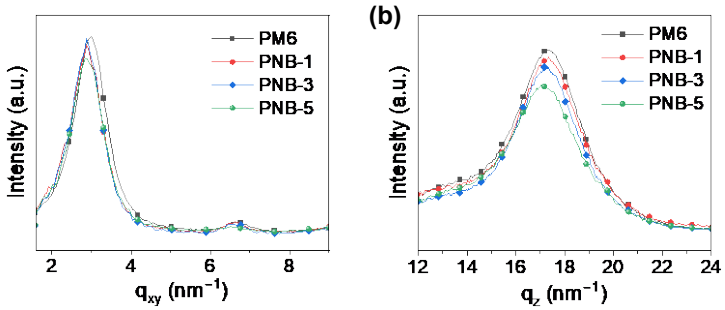

Figure S4. a) (100) diffraction peaks of the polymers. b) (010) diffraction peaks of the polymers.

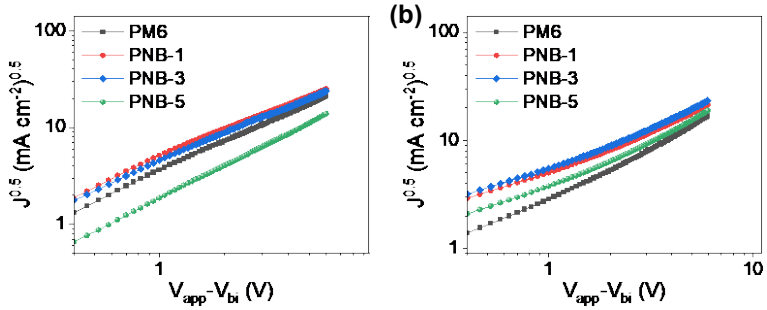

Figure S5. $J^{0.5}$-V curves of the (a) hole-only and (b) electron-only devices based on various active blends.

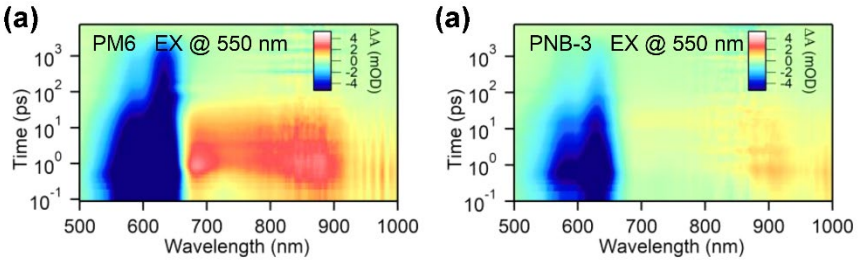

Figure S6. Color plots offs-TAS of various films: a) L8-BO, b) PNB-3.

4. Supplementary Tables

Table S1. Summarized photovoltaic parameters of the reported random terpolymer-based binary OSCs using Y6 derivatives as the acceptor.

Active blend	V_{oc} [V]	J_{sc} [mA cm^{-2}]	FF [%]	PCE [%]	Reference
DTTz-20:BTP-eC9	0.86	25.21	73.2	16.37	[2]
PMT-CT-10:Y6	0.83	28.12	77.9	18.21	[3]
DEH-20:L8-BO	0.907	22.4	71.6	14.6	[4]
PM6-TzBI-10:L8-BO	0.897	25.63	79.84	18.36	[5]
PBNB80:BO-4Cl	0.849	25.6	71.8	15.6	[6]
DM1:Y6	0.85	25.86	78.29	17.21	[7]
PFBT4T-T20:Y14	0.79	26.56	74.34	15.6	[8]
H6:Y6	0.888	26.51	76.98	18.12	[9]
D18-20%Cl:Y6	0.861	27.20	78.06	18.28	[10]
PM6-DCNBT-10:L8-BO	0.902	25.77	77.50	18.01	[11]
SZ13:Y6	0.82	26.25	70.65	15.28	[12]
PTQ10 90:10/Y6	0.81	25.5	68	13.8	[13]
SZ22–0.2:Y6	0.83	25.78	73.39	15.64	[14]
PMZ2:Y6	0.854	26.9	77.2	17.8	[15]
PL1:BTP-eC9-4F	0.876	27.11	76.41	18.14	[16]

OPz11:Y6	0.865	27.02	78.71	18.42	[17]
PF1:Y6	0.87	26.3	76	17.3	[18]
PM6-Si30:BTP-eC9	0.887	24.69	65.37	14.32	[19]
PBET10:Y6-BO	0.87	25.19	68.02	14.95	[20]
PCE10-BDT2F-0.8:Y6	0.753	26.36	69.45	13.80	[21]
PM6Ir1:Y6	0.848	26.16	75.33	16.71	[22]
PM6Ir1:N3	0.84	26.13	74.11	16.27	[23]
PM6-Ir1.5:Y6-C2	0.839	26.09	77.98	17.09	[24]
PM6-Ir1:Y6	0.845	26.15	78.40	17.32	[25]
PMZ-10:Y6	0.834	27.96	78.2	18.23	[26]
PM6-T15:Y6	0.86	27.02	71.14	16.61	[27]
TP-H:Y6	0.851	26.78	73.53	16.76	[28]
P75:Y6	0.81	22.6	58	10.28	[29]
PBDB-TF-T10:Y6	0.84	27.9	70	16.4	[30]
PM6-SiCl-10%:Y6	0.870	25.37	73.48	16.22	[31]
OPz1:Y6	0.871	25.34	73.7	16.28	[32]
PM1:Y6	0.87	25.9	78	17.6	[33]
PFBCNT20:Y6-BO	0.84	26.3	73.9	16.3	[34]
PBDB-ThCl15:Y6	0.84	25.21	74.03	15.63	[35]
PM20Si: Y6	0.80	26.75	70.01	14.95	[36]
S1:Y6	0.877	25.40	73.7	16.42	[37]
PL-1:Y6	0.82	25.57	78.1	16.37	[38]
PMD-15:L8-BO	0.904	25.90	77.39	18.12	[39]

Table S2. Charge carrier mobilities of the various type OSCs.

Polymer	E_g [eV]	V_{oc} [V]	$V_{oc,SQ}$ [V]	$V_{oc,rad}$ [V]	ΔE_1 [eV]	ΔE_2 [eV]	ΔE_3 [eV]	E_{loss} [eV]
PM6	1.440	0.893	1.173	1.105	0.267	0.068	0.212	0.547
PNB-1	1.440	0.903	1.173	1.106	0.267	0.067	0.203	0.537
PNB-3	1.440	0.907	1.173	1.106	0.267	0.067	0.199	0.533
PNB-5	1.445	0.914	1.178	1.112	0.267	0.066	0.198	0.531

Table S3. Charge carrier mobilities of the various type OSCs.

Active layer	μ_h [$\times 10^{-4}$ cm^2 V^{-1} s^{-1}]	μ_e [$\times 10^{-4}$ cm^2 V^{-1} s^{-1}]	μ_h/μ_e
PM6:L8-BO	4.07	2.95	1.38
PNB-1:L8-BO	4.76	3.64	1.31
PNB-3:L8-BO	4.52	4.37	1.03
PNB-5:L8-BO	2.21	3.42	1.55

5. References

[1] Y. Li, H. Meng, T. Liu, Y. Xiao, Z. Tang, B. Pang, Y. Li, Y. Xiang, G. Zhang, X. Lu, G. Yu, H. Yan, C. Zhan, J. Huang, J. Yao, *Adv. Mater.* **2019**, *31*, 1904585.

[2] C. Lim, S. Lee, D. Han, C. Lee, B. J. Kim, *Macromolecules* **2022**, *55*, 10395.

[3] L. Zhou, L. Meng, J. Zhang, S. Qin, J. Zhang, X. Li, J. Li, Z. Wei, Y. Li, *Adv. Sci.* **2022**, *9*, 2203513.

[4] Y. Luo, X. Wang, M. Zhang, X. Sun, A. Saparbaev, S. Lei, J. Zhang, B. Xiao, C. Yang, Z. Liu, R. Yang, *Solar RRL* **2022**, *6*, 2200679.

[5] T. Y. Yang, C. T. Liao, Y. W. Duan, X. P. Xu, M. Deng, L. Y. Yu, R. P. Li, Q. Peng, *Adv. Funct. Mater.* **2022**, DIO: 10.1002/adfm.202208950.

[6] T. Zhang, C. An, Q. Lv, J. Qin, Y. Cui, Z. Zheng, B. Xu, S. Zhang, J. Zhang, C. He, J. Hou, *J. Energy Chem.* **2021**, *59*, 30.

[7] X. Deng, Y. Fang, B. Huang, F. Liao, K. Liu, J. Zhang, S. Chen, S. Kim, C. Yang, D. Ye, J. Liu, L. Chen, *Chem. Commun.* **2022**, *58*, 11823.

[8] J. Liang, S. Lei, L. Zhang, F. Pan, M. Luo, H. Liu, Z. Zhang, D. Yuan, J. Chen, *ACS Appl. Energy Mater.* **2022**, *5*, 11866.

[9] B. Huang, X. Deng, H. Jin, K. Liu, S. Chen, Z. Ma, J. Oh, C. Yang, J. Liu, L. Chen, *J. Mater. Chem. A* **2022**, *10*, 18714.

[10] H.-R. Bai, Q. An, H.-F. Zhi, M. Jiang, A. Mahmood, L. Yan, M.-Q. Liu, Y.-Q. Liu, Y. Wang, J.-L. Wang, *ACS Energy Lett.* **2022**, *7*, 3045.

[11] J. J. Shao, C. T. Liao, X. P. Xu, M. Deng, L. Y. Yu, R. P. Li, Q. Peng, *Chem. Mater.* **2022**, *34*, 7971.

[12] X. Jing, Y. Zhao, Q. Wang, X. Kang, X. Liu, X. Wang, L. Yu, M. Sun, *Dyes Pigments* **2022**, *206*, 110609.

[13] A. L. Jones, C. H. Y. Ho, S. A. Schneider, J. Zhang, Y. Pei, J. Wang, X. Zhan, S. R. Marder, M. F. Toney, F. So, G. N. Manjunatha Reddy, J. R. Reynolds, *Chem. Mater.* **2022**, *34*, 6853.

[14] X. Jing, Y. Zhao, Q. Wang, X. Kang, T. Zhuang, X. Liu, X. Wang, L. Yu, M. Sun, *Polymer* **2022**, *254*, 125089.

[15] J. Wu, X. Guo, M. Xiong, X. Xia, Q. Li, J. Fang, X. Yan, Q. Liu, X. Lu, E. Wang, D. Yu, M. Zhang, *Chem. Eng. J.* **2022**, *446*, 137424.

[16] H. Lu, H. Wang, G. L. Ran, S. Li, J. Q. Zhang, Y. H. Liu, W. K. Zhang, X. J. Xu, Z. S. Bo, *Adv. Funct. Mater.* **2022**, *32*, 2203193.

[17] Z. Liao, D. Hu, H. Tang, P. Huang, R. Singh, S. Chung, K. Cho, M. Kumar, L. Hou, Q. Chen, W. Yu, H. Chen, K. Yang, Z. Kan, F. Liu, Z. Xiao, G. Li, S. Lu, *J. Mater. Chem. A* **2022**, *10*, 7878.

[18] Q. Guo, J. Lin, X. Dong, L. Zhu, X. Guo, F. Liu, M. Zhang, *Chem. Eng. J.* **2022**, *431*, 134117.

[19] W. Peng, Y. Lin, S. Y. Jeong, Z. Genene, A. Magomedov, H. Y. Woo, C. Chen, W. Wahyudi, Q. Tao, J. Deng, Y. Han, V. Getautis, W. Zhu, T. D. Anthopoulos, E. Wang, *Nano Energy* **2022**, *92*, 106681.

[20] J. Kim, M. Kyeong, J.-W. Ha, H. Ahn, J. Jung, S. Seo, T. N.-L. Phan, C. Lee, S. C. Yoon, B. J. Kim, S.-J. Ko, *J. Mater. Chem. A* **2021**, *9*, 27551.

[21] X. Huang, L. Zhang, Y. Cheng, J. Oh, C. Li, B. Huang, L. Zhao, J. Deng, Y. Zhang, Z. Liu, F. Wu, X. Hu, C. Yang, L. Chen, Y. Chen, *Adv. Funct. Mater.* **2021**, *32*, 2108634.

[22] M. Zhang, X. Ma, H. Zhang, L. Zhu, L. Xu, F. Zhang, C.-S. Tsang, L. Y. S. Lee, H. Y. Woo, Z. He, W.-Y. Wong, *Chem. Eng. J.* **2022**, *430*, 132832.

[23] S. Zhang, M. Zhang, X. Wang, C. Xu, W. Xu, J. Gao, J. Wang, W.-Y. Wong, J. H. Son, S. Y. Jeong, H. Y. Woo, F. Zhang, *Sustain. Energy Fuels* **2021**, *5*, 5825.

[24] R. Sun, T. Wang, Z. Luo, Z. Hu, F. Huang, C. Yang, J. Min, *Solar RRL* **2020**, *4*, 2000156.

[25] T. Wang, R. Sun, M. Shi, F. Pan, Z. Hu, F. Huang, Y. Li, J. Min, *Adv. Energy Mater.* **2020**, *10*, 2000590.

[26] L. Zhou, L. Meng, J. Zhang, C. Zhu, S. Qin, I. Angunawela, Y. Wan, H. Ade, Y. Li, *Adv. Funct. Mater.* **2021**, *32*, 2109271.

[27] S. Tu, L. Zhang, X. Lin, L. Xiao, W. Wang, Q. Ling, *J. Mater. Chem. C* **2022**, *10*, 2026.

[28] L. Xu, W. Tao, M. Guan, X. Yang, M. Huang, H. Chen, J. Zhang, B. Zhao, S. Tan, *ACS Appl. Energy Mater.* **2021**, *4*, 11624.

[29] J. J. Ji, J. Q. Xie, J. H. Tang, K. B. Zheng, Z. Q. Liang, *Solar RRL* **2021**, *5*, 2100142.

[30] Y. Xu, Q. Ji, L. Yin, N. Zhang, T. Liu, N. Li, X. He, G. Wen, W. Zhang, L. Yu, P. Murto, X. Xu, *ACS Appl. Mater. Interfaces* **2021**, *13*, 23993.

[31] Y. Cheng, H. Jin, J. Oh, X. Huang, R. Lv, B. Huang, Z. Ma, C. Yang, L. Chen, Y. Chen, *J. Mater. Chem. A* **2021**, *9*, 9238.

[32] Z. H. Liao, K. Yang, L. C. Hou, J. Li, J. Lv, R. Singh, M. Kumar, Q. Q. Chen, X. Y. Dong, T. L. Xu, C. Hu, T. N. Duan, Z. P. Kan, S. R. Lu, Z. Y. Xiao, *Macromolecules* **2020**, *53*, 9034.

[33] J. Wu, G. Li, J. Fang, X. Guo, L. Zhu, B. Guo, Y. Wang, G. Zhang, L. Arunagiri, F. Liu, H. Yan, M. Zhang, Y. Li, *Nat. Commun.* **2020**, *11*, 4612.

[34] Y. Zhang, L. Pan, Z. Peng, W. Deng, B. Zhang, X. Yuan, Z. Chen, L. Ye, H. Wu, X. Gao, Z. Liu, C. Duan, F. Huang, Y. Cao, *J. Mater. Chem. A* **2021**, *9*, 13522.

[35] M. Pu, H. Chen, P. Chao, Y. Zhu, N. Zheng, H. Lai, T. Zhao, F. He, *ACS Appl. Polym. Mater.* **2020**, *3*, 14.

[36] W. Xu, M. Zhang, J. Xiao, M. Zeng, L. Ye, C. Weng, B. Zhao, J. Zhang, S. Tan, *Polym. Chem.* **2020**, *11*, 6178.

[37] H. L. Sun, T. Liu, J. W. Yu, T. K. Lau, G. Y. Zhang, Y. J. Zhang, M. Y. Su, Y. M. Tang, R. J. Ma, B. Liu, J. E. Liang, K. Feng, X. H. Lu, X. G. Guo, F. Gao, H. Yan, *Energy Environ. Sci.* **2019**, *12*, 3328.

[38] X. Li, R. Ma, T. Liu, Y. Xiao, G. Chai, X. Lu, H. Yan, Y. Li, *Sci. China Chem.* **2020**, *63*, 1256.

[39] X. Chen, C. Liao, M. Deng, X. Xu, L. Yu, R. Li, Q. Peng, *Chem. Eng. J.* **2023**, *451*, 139046.